Phase transformation in multiferroic Bi5Ti3FeO15 ceramics by temperature-dependent ellipsometric and Raman spectra: An interband electronic transition evidence

P. P. Jiang, Z. H. Duan, L. P. Xu, X. L. Zhang, Y. W. Li, Z. G. Hu, and J. H. Chu

Citation: Journal of Applied Physics **115**, 083101 (2014); doi: 10.1063/1.4866421
View online: http://dx.doi.org/10.1063/1.4866421
View Table of Contents: http://scitation.aip.org/content/aip/journal/jap/115/8?ver=pdfcov
Published by the AIP Publishing

Phase transformation in multiferroic $Bi_5Ti_3FeO_{15}$ ceramics by temperature-dependent ellipsometric and Raman spectra: An interband electronic transition evidence

P. P. Jiang (姜鹏鹏), Z. H. Duan (段志华), L. P. Xu (徐丽萍), X. L. Zhang (张小龙), Y. W. Li (李亚巍), Z. G. Hu (胡志高),[a] and J. H. Chu (褚君浩)
Key Laboratory of Polar Materials and Devices, Ministry of Education, Department of Electronic Engineering, East China Normal University, Shanghai 200241, China

(Received 12 December 2013; accepted 9 February 2014; published online 24 February 2014)

Thermal evolution and an intermediate phase between ferroelectric orthorhombic and paraelectric tetragonal phase of multiferroic $Bi_5Ti_3FeO_{15}$ ceramic have been investigated by temperature-dependent spectroscopic ellipsometry and Raman scattering. Dielectric functions and interband transitions extracted from the standard critical-point model show two dramatic anomalies in the temperature range of 200–873 K. It was found that the anomalous temperature dependence of electronic transition energies and Raman mode frequencies around 800 K can be ascribed to intermediate phase transformation. Moreover, the disappearance of electronic transition around 3 eV at 590 K is associated with the conductive property. © *2014 AIP Publishing LLC*. [http://dx.doi.org/10.1063/1.4866421]

I. INTRODUCTION

In recent years, the Aurivillius family of bismuth layer structured compounds with general formula $(Bi_2O_2)^{2+}(A_{n-1}B_nO_{3n-1})^{2-}$ has attracted much attention due to the remarkable multiferroic, lead/fatigue-free characteristics and high Curie temperature (T_c). These excellent properties make it potential applications as non-volatile ferroelectric random access memories (FeRAMs) and high-temperature piezoelectric materials.[1,2] Among them, $Bi_5Ti_3FeO_{15}$ (BTF) is one of such compounds for $n=4$, which is ferroelectromagnetic in nature. It has a four-layered unit of nominal perovskite-like $(Bi_3Ti_3FeO_{13})^{2-}$ sandwich by two fluoride-like $(Bi_2O_2)^{2+}$ layers.[3] Recent studies indicate that it is of ferroelectricity with T_c of about 1023 K and antiferromagnetic with Néel point of about 80 K, respectively.[4]

Up to date, there have been intensive studies on ferroelectric transformation for the Aurivillius family. It was found that the odd-layered compounds present a single structural transition, while many even-layered compounds exhibit two consecutive phase transitions ($n \leq 4$). For the odd-layered material, $Bi_4Ti_3O_{12}$ ($n=3$) shows an avalanche transformation (single ferroelectric-paraelectric (FE-PE)-paraelectric (PE) transformation).[5,6] For the even-layered compounds, $Sr_{0.85}Bi_{2.1}Ta_2O_9$ ($n=2$) and $SrBi_4Ta_4O_{15}$ ($n=4$), an intermediate PE orthorhombic (*Amam*) phase was revealed between FE orthorhombic ($A2_1am$) phase and PE tetragonal (*I*4/*mmm*) phase by high-temperature neutron powder diffraction (HT-NPD).[7,8] The phenomena are widely accepted because the symmetry of the FE phase in all these compounds cannot be explained by only considering the symmetric break due to the FE distortion.[6] Unfortunately, such consecutive transformations seem to be absent in other analogous members of the Aurivillius family. It was recently reported that BTF and $SrBi_2Nb_2O_9$ ($n=2$) exhibited only a single-step structural transformation ($A2_1am$ to *I*4/*mmm*) by HT-NPD.[9,10] However, birefringence data for BTF system indicated the existence of the intermediate PE orthorhombic phase.[11]

Hence, whether an intermediate phase (e.g. space group *Amam*) exists between FE orthorhombic and PE tetragonal phase in BTF ceramic is still an open issue. Moreover, knowledge of temperature-dependent complex dielectric functions and phonon modes is important to understand the origin of lattice instabilities and phase transformations. It is required for the application as a dielectric material. Nevertheless, few reports about thermal-optical responses and lattice vibrations of BTF ceramic have been presented up to now. Spectroscopic ellipsometry (SE) is a suitable and nondestructive technique for directly measuring the complex dielectric functions $\tilde{\varepsilon}(\omega) = \varepsilon_1 + i\varepsilon_2$.[12] As we know, the complex dielectric functions are intrinsically associated with energy band structures and electronic transitions. Moreover, some obvious variations of optical constants can be caused by structural changes during phase transformations.[13,14] On the other hand, Raman scattering can provide some invaluable information on lattice vibrations and structural variations. Thus, one would expect that the phase/structural transformation can be clarified by interband electronic transition and/or phonon mode variation with the temperature.

In this article, variable-temperature SE and Raman scattering are applied to further investigate the intrinsical physical behaviors of BTF ceramic. The intermediate phase transformation, interband transitions, and phonon modes have been discussed in detail.

II. EXPERIMENTAL DETAILS

Aurivillius BTF ceramic was synthesized using a conventional solid state reaction method. The TiO_2, Fe_2O_3, and Bi_2O_3 powders as precursor materials with 3 wt. % excess Bi_2O_3 to compensate the Bi volatilization were ball milled

[a]Author to whom correspondence should be addressed. Electronic mail: zghu@ee.ecnu.edu.cn. Tel.: +86-21-54345150. Fax: +86-21-54345119.

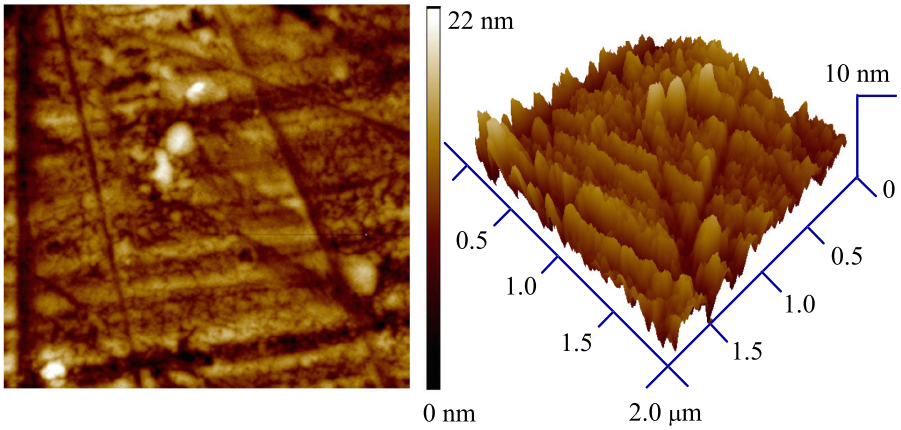

FIG. 1. The two-dimensional and three-dimensional AFM surface morphology of BTF ceramic. Note that the scanning area is $2 \times 2\ \mu m^2$.

together in ethanol for 24 h, presintered at 800 °C for 6 h, and then ball milled again for 24 h. Finally, the pretreated powders were pressed into small pellets and sintered at 1050 °C for 240 min. The details of fabricating process can be found in Ref. 15. Before spectral measurements, the ceramic was rigorously double-side polished and cleaned in pure ethanol with an ultrasonic bath and rinsed several times by deionized water. The phase and crystal structure of BTF ceramic were determined by X-ray diffraction (XRD) using Cu $K\alpha$ radiation (D/MAX-2550 V, Rigaku Co.), which indicates that the BTF ceramic is polycrystalline without any impurity phases at room temperature (RT). The surface morphology of the BTF ceramic was examined by atomic force microscopy (AFM: Digital Instruments Icon, Bruker). Temperature-dependent SE experiments were performed in the photon energy region from 1.12 to 6.52 eV. The spectral resolution is set to 5 nm and the incident angle is fixed to 70° by a vertical variable-angle SE (J. A. Woollam Co., Inc.). The BTF ceramic was mounted into an Instec cell by the clamping way. The window effect can be eliminated through the calibration taking silicon sample. The spectral data were recorded with the auto retarder (high accuracy). The temperature can be varied from 200 to 873 K with the interval of 15 K and the set-point stability is better than 1 K. In addition, temperature-dependent Raman scattering measurements were carried out by a Jobin-Yvon LabRAM HR UV micro-Raman spectrometer. The He-Ne laser with the wavelength of 632.8 nm is taken as the exciting source. The temperature variation from 200 to 873 K was controlled by a Linkam THMSE 600 heating/cooling stage with a precision of about 0.5 K.

III. RESULTS AND DISCUSSION

Fig. 1 illustrated the AFM surface morphology of BTF ceramic, which was observed after the high-temperature ellipsometric measurements. One can see that the surface is dense, smooth, and uniform without cracks. Especially, the root-mean-square (RMS) surface roughness is estimated to be about 2.8 nm. In the present work, a three-layer model (air/surface roughness/ceramic) was used to evaluate the complex dielectric functions of BTF ceramic and the thickness of roughness layer. Brüggeman effective-medium approximation (EMA) with a mixture of the bulk material (50%) and voids (50%) was applied to model the surface roughness layer. Three parametric oscillators, two Psemi-M0 models and one Psemi-M3 model, were applied to estimate the complex dielectric functions lower than 590 K while two parametric oscillators, Psemi-M0 and Psemi-M3, were applied to estimate the complex dielectric functions beyond 590 K.[16] The comprehensive values of the parameters for the fitted spectra obtained at 200/590 K are listed in Table I. The fitting procedure was carried out with WVASE32 software package (J.A. Woollam Co., Inc.).

The well-fitted complex dielectric functions at 200 and 590 K are plotted in Figs. 2(b) and 2(c). The accurate thickness of the roughness layer is about 2.9 nm, which agrees well with the result of AFM. The real and imaginary parts of the modeled complex dielectric functions for BTF ceramic at some typical temperatures are plotted in Fig. 2(a). Note that the value of ε_2 (about 6) at 4 eV is larger than the data (about 4) reported in Ref. 15. Nevertheless, the complex dielectric functions are obtained without considering the surface roughness in Ref. 15. In the present work, the maximum value of ε_2 extracted from the optical model is about 1.0

TABLE I. The well-fitting parameter values for BTF ceramic at 200/590 K. The parameter *A*, *E*, *B*, *WL*, *WR*, *PL*, *PR*, *AL*, *AR*, *O2L*, and *O2R* is amplitude, center energy, broadening, width of left side absorption region, width of right side absorption region, control point position for left side, control point position for right side, control point amplitude for left side, control point amplitude for right side, second order polynomial factor for left side polynomials, and second order polynomial factor for right side polynomials, respectively. The label "-" means that the parameter is fixed during the fitting process.

	Parameters	*A*	E_0 (eV)	*B* (eV)	*WR* (eV)	*WL* (eV)	*PR*	*PL*	*AR*	*AL*	*O2R*	*O2L*	ε_0 offset
200 K	PSM3.0	17.4	5.1	0.8	–	2.9	0.5	0.1	–	0.03	–	0.21	2.3
	PSM0.0	1.9	3.6	0.2	5.1	–	0.3	–	2.9	–	−0.8	–	
	PSM0.0	36.2	0.3	0.2	2.3	–	0.07	–	0.01	–	−0.4		
590 K	PSM3.0	19.4	5.0	0.8	–	1.3	–	0.1	–	0.03	–	1.0	1.95
	PSM0.0	2.3	3.5	0.3	6.0	–	0.3	–	3.2	–	−0.8	–	

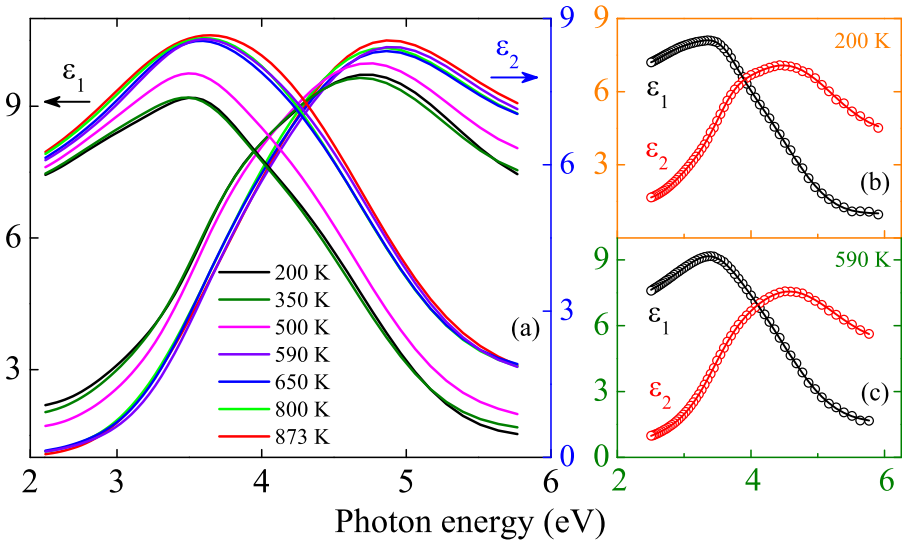

FIG. 2. (a) The real (ε_1) and imaginary (ε_2) parts of the modeled complex dielectric functions for BTF ceramic at several typical temperatures. (b)–(c) The experimental data (dots) and best-fit curves (solid lines) of the complex dielectric functions at 200 and 590 K, respectively.

greater than the original data. The discrepancy is mainly due to the effect from the surface roughness. Thus, one can conclude that both of them are reasonable due to different surface roughness. Moreover, the maximum value of ε_2 is slightly larger than 6 for the most typical perovskite structural materials (such as $LiNbO_3$, $SrTiO_3$, $BaTiO_3$).[17] It indicates that the present data agree well with other perovskite oxides. It should be emphasized that the BTF ceramics have the same microstructure after and before the heating experiment (not shown). The sharpening variation of the dielectric function observed could be intrinsically due to the temperature effects. As we can see, the parameter ε_2 in the low-energy region decreases with the temperature. The maximum value of ε_2 at about 4.6 eV increases due to the red shift of interband transition energies. Meanwhile, the value of ε_1 starts at about 7 and first approaches a peak at 3.5 eV and then deceases due to the well-known Van Hove singularities. The parameter ε_2 in the low-energy region decreases with the temperature which is contrary to the result of temperature-dependent ε_2 for semiconductor silicon.[18] The phenomena can be ascribed to the band tail states forming near the conduction band which is induced by the oxygen (O) and bismuth (Bi) vacancies. The electrons in the band tail state are mainly excited by the photon in the relatively low temperatures. However, the electronic transitions are gradually caused by thermal activation with increasing the temperature. Therefore, the above phenomena on the downtrend of ε_2 in the low-energy region can be reasonably explained.

In order to study the temperature evolution of interband transitions, a line-shape analysis with standard critical point (SCP) model was performed, which has been successfully applied in semiconductors and ferroelectric materials. The real and imaginary parts of the second derivative of dielectric functions with respect to photon energy ($d^2\varepsilon/dE^2$) were simultaneously fitted using a least-squares procedure. Note that the $d^2\varepsilon/dE^2$ values were directly calculated by the original data because the surface roughness layer mainly affects the transition intensity other than the center energy. The process can be effective on BTF ceramic because the difference of complex dielectric functions is not obvious whether the surface roughness is considered or not. Moreover, it can better obtain the real values and thermal evolution of critical points with avoiding the errors introduced by the artificial fitting process.[14] The experimental second-derivative spectra of the dielectric functions at 200, 575, 590, and 873 K are shown in Fig. 3. The solid lines represent the best fits to the SCP model written as follows:[18]

$$\frac{d^2\varepsilon}{dE^2} = \begin{cases} j(j-1)A_m e^{i\Phi_m}(E - E_m + i\Gamma_m)^{j-2}, & j \neq 0 \\ A_m e^{i\Phi_m}(E - E_m + i\Gamma_m)^{-2}, & j = 0. \end{cases} \quad (1)$$

where A_m, Φ_m, Γ_m, and E_m denote the amplitude, the phase angle, the broadening, and the threshold energy, respectively. The parameter m represents the number of oscillators used in the fitting process. The exponent j has the values of -1, -0.5, 0, and 0.5 for excitonic, one-, two-, and three-dimensional line shapes, respectively. For example, the parameter values from the SCP model at different temperatures are listed in Table II. Three critical points around 3, 3.7, and 4.6 eV can be well observed, which are labeled by E_1, E_2, and E_3, respectively. The physical origin of E_1 transition can

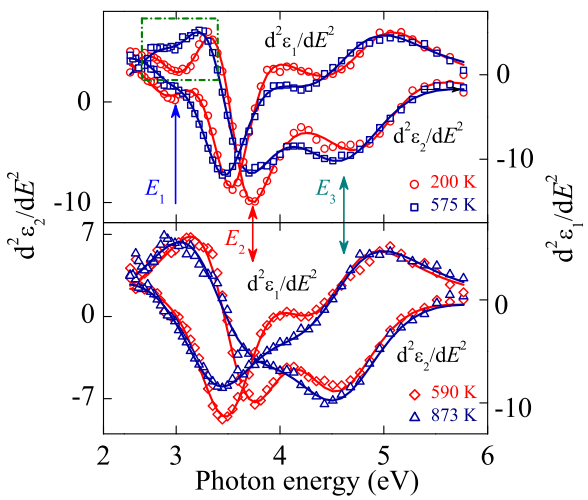

FIG. 3. The experimental data (dots) and best-fit curves (solid lines) for the second derivatives of the dielectric functions from BTF ceramic at 200, 575, 590, and 873 K, respectively.

TABLE II. Parameter values of the SCP model for BTF ceramic are extracted from the best-fitting (Figure 3) at 200, 575, 590, and 873 K, respectively. Note that the 95% reliability of the fitting parameters is given in parentheses.

Temperature (K)	200			575			590			873		
Parameters	E_1	E_2	E_3	E_1	E_2	E_3	E_1	E_2	E_3	E_1	E_2	E_3
A	1.29	2.25	4.38	0.56	2.97	6.20	–	4.55	5.01	–	5.47	6.91
	(0.55)	(0.07)	(1.80)	(0.04)	(0.54)	(0.81)	–	(1.08)	(0.41)	–	(1.79)	(2.02)
Φ (deg)	38.3	38.6	40.7	38.6	38.4	40.2	–	38.9	39.8	–	38.2	40.1
	(0.34)	(0.09)	(0.17)	(0.33)	(0.08)	(0.28)	–	(0.06)	(0.10)	–	(0.09)	(0.09)
E (eV)	2.90	3.55	4.87	2.96	3.44	4.63	–	3.54	4.51	–	3.34	4.56
	(0.09)	(0.02)	(0.02)	(0.05)	(0.02)	(0.09)	–	(0.02)	(0.04)	–	(0.03)	(0.02)
Γ (eV)	0.55	0.44	0.84	0.48	0.53	0.95	–	0.64	0.82	–	0.81	0.96
	(0.11)	(0.01)	(0.13)	(0.38)	(0.03)	(0.09)	–	(0.06)	(0.04)	–	(0.10)	(0.08)

be ascribed to a charge transfer (CT) transition to a low-lying electronic structure forming on the tail of the optical energy band gap E_2. As we can see, E_1 transition gradually degraded and finally disappeared at about 590 K due to the disappearance of photon-excited electronic transition. The transition E_2 is assigned to the dipole-allowed CT transition.[19] The transition is a directly allowed optical transition between the valence and conduction bands from O 2*p* states to titanium (Ti) 3*d* states.[15,20] The valence-band maximum is predominantly constituted of the O 2*p* and ferrum (Fe)/Ti 3*d* states. The conduction-band minimum is a mixture of Fe/Ti 3*d*, O 2*p* and Bi 6*p* states.[21] Moreover, the transition E_3 mainly originates from both the *d-d* and *p-d* CT transitions in octahedral Ti/FeO_6 centers. Both E_2 and E_3 transitions present a distinct temperature-dependence lower than/beyond 800 K. The anomalies can be ascribed to the intermediate phase transformation.

Next, the thermal evolution of interband electronic transition energies for BTF ceramic is plotted in Fig. 4. The parameters E_2 and E_3 show a typically red shift trend with the temperature and E_1 energy remains nearly unchanged at 2.95 eV lower than 590 K. Generally, the disappearance of E_1 optical transition can be explained by the fact that the

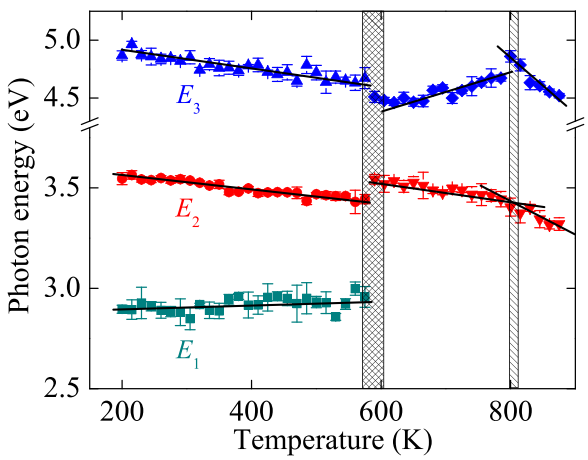

FIG. 4. Temperature dependence of interband electronic transition energies for BTF ceramic. The left striation indicates E_1 transition disappears around 575 K while the right striation shows the phase transformation around 800 K.

electronic transitions to the band tail states by photon excitation are replaced by thermal activation. When a certain amount of electrons are activated to the band tail state, these electrons can be activated to the conduction band through photon absorption promptly. The disappearance of the E_1 transition is associated with the conductive properties of BTF ceramic. The result agrees well with the temperature dependence of dielectric constants and dielectric loss, which showed an obvious increase at about 673 K.[22] It was reported that electronic structural variations induced by phase transformation can be associated with the distinct variation of electronic transition energies and the complex dielectric functions.[14] For E_2 transition, the value gradually shifts to a lower energy from 3.54 to 3.40 eV in the temperature range from 590 to 800 K. The temperature coefficient of E_2 (about -1×10^{-3} eV/K) beyond 800 K is much lower than the slope (about -5×10^{-4} eV/K) between 590 K and 800 K. For E_3 transition, the value first increases from 4.50 to 4.86 eV in the temperature range of 590–800 K and then decreases to 4.55 eV. These abnormal changes could be ascribed to the structural distortion induced by the intermediate phase transformation, as discussed in the following Raman scattering. The existence of the intermediate phase transformation is consistent with the basic paradigm from the Landau theory of structural phase transformations for BTF ceramic.[6] It predicts that the final symmetric structure can be explained by two symmetry-breaking modes in BTF ceramic. Because the simultaneous freezing of such two independent modes is scarce, it is difficult to directly explain phase transformation from FE orthorhombic phase to PE tetragonal phase without an intermediate phase. Hence, it is reasonable to consider the anomalies as an intermediate FE-PE phase transformation before the ferroelectric transformation at 1023 K, which is necessary for the condensation of the two modes.[6] It was reported that two endothermic peaks was found at 793 and 1073 K by the thermal analysis, which agrees well with the present results.[23] The ellipsometric analysis confirms the interesting phenomena and explains the intermediate phase transformation.

Correspondingly, Fig. 5(a) presents Raman spectra of BTF ceramic in the temperature range from 200 to 873 K. Note that all Raman spectra were corrected for the Bose-Einstein temperature factor to eliminate the contribution from

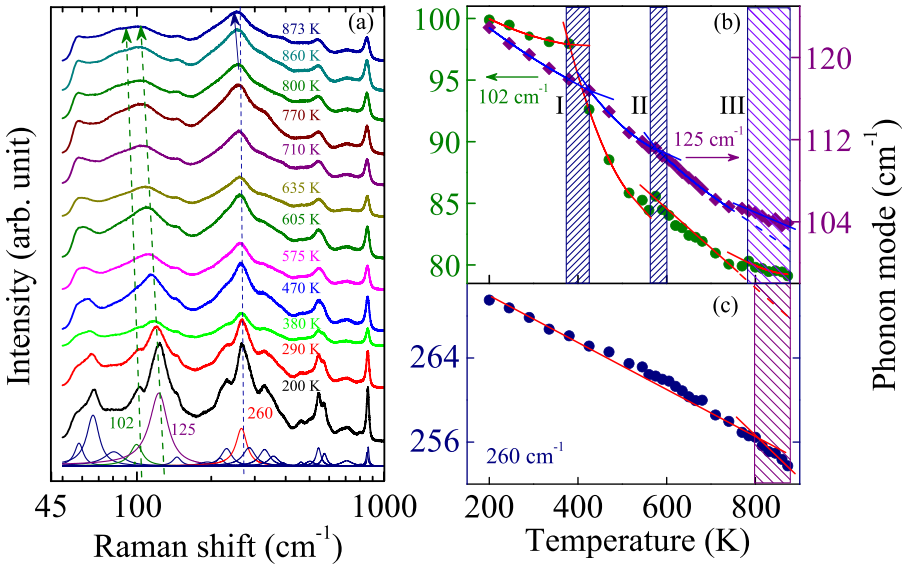

FIG. 5. (a) Temperature-dependent Raman scattering for BTF ceramic from 200 to 873 K. (b) The variation of phonon modes 102 an 125 cm^{-1} related to the vibration of Bi atoms in the perovskitelike slabs with the temperature. (c) The variation of phonon mode 260 cm^{-1} with the temperature, which is associated with the torsional bending of Ti/FeO_6 octahedra. Note that the fitting to the Lorentzian functions is presented in (a).

the Bose Einstein population factor.[24] Figs. 5(b) and 5(c) show the details on thermal evolution of some typical Raman modes at 102, 125, and 260 cm^{-1}, respectively. Note that the mode at 60 cm^{-1} was added to correct the influence of instrumental artefact. The mode located at about 66 cm^{-1} with A_{1g} character is related to the displacement of Bi^{3+} ions within the Bi_2O_2 layers.[25] It is insensitive to the temperature according to the weak red shift. The modes located at 99 cm^{-1} and 122 cm^{-1} are associated with the motion of Bi cations in the perovskitelike slabs.[25] On the other hand, the internal vibrations of Ti/FeO_6 octahedra occur above 200 cm^{-1} because the intragroup binding energy within the Ti/FeO_6 octahedra is much larger than the intergroup and/or crystal binding energy.[26] Therefore, the high frequency modes at 256 and 864 cm^{-1} are associated with the torsional bending and stretching behaviors of Ti/FeO_6 octahedra, respectively. In Fig. 5(b), the modes at 99 cm^{-1} and 122 cm^{-1} gradually shift to 79 cm^{-1} and 103 cm^{-1} with increasing the temperature, respectively. It is more easily disturbed by temperature as compared to the Bi atoms within the Bi_2O_2 layers. The red shift of these modes can be usually explained by thermal expansion of the lattice and anharmonic phonon-phonon interactions.[27] The anomalies III in temperature dependence of Raman modes agree well with evolution of interband optical transitions observed by ellipsometry. Note that the vibrations of Bi atoms become more easily disturbed beyond 380 K according to the distinct down trend, which is caused by the change of bond distances between the Bi atoms within Bi_2O_2 layer and the apical O atoms of the perovskitelike block. The bond distances are split from two different distances into four different distances beyond 380 K.[10] Moreover, the region II is in according with the missing of optical transition E_1 at about 590 K. It seems that the disappearance of the E_1 transition has little influence on structural vibrations.

In general, a phase transformation can be driven by various combinations of displacive modes. It is known that the displacement of Bi atoms along *a*-axis with respect to the chains of BO_6 octahedra is closely related to the ferroelectricity.[8] As we can see in Fig. 5(b), both of the related modes show different trends beyond about 800 K. Furthermore, in Fig. 5(c), the mode at 260 cm^{-1} with A_{1g}[Ti] character presents a more remarkable red shift beyond 800 K. The anomalous temperature dependence of the aforementioned phonon modes along with the anomalies of electronic transitions (E_2, E_3) observed around 800 K indicates the existence of intermediate phase transformation. It is worthy to note that the modes related to Bi atom vibrations feel the phase transformation a bit earlier than the mode associated with torsional bending of Ti/FeO_6 octahedra. The case is because the bending of Ti/FeO_6 octahedra can be first disturbed by the Bi atom vibration in the perovskite-like slabs, which finally results in the intermediate FE-PE phase transformation. Note that the structural change of the intermediate phase transition is relatively weak when compared to the following ferroelectric phase transition at 1023 K, which usually can be ignored by simply structural analysis. Fortunately, combined with the remarkable anomalies on the thermal evolution of electronic transition energies, the anomalies in the temperature dependence of Raman modes can be well revealed.

IV. SUMMARY

In summary, thermal evolution behaviors of $Bi_5Ti_3FeO_{15}$ ceramic have been investigated by spectroscopic ellipsometry and Raman scattering in the temperature range of 200–873 K. An intermediate FE orthorhombic to PE orthorhombic phase transformation is determined at about 800 K. This work gives invaluable information on three interband electronic transitions and structural evolution for BTF ceramic. Moreover, it provides an effective method to study the Aurivillius family, which has controversy on the intrinsic mechanism of the intermediate phase transformation.

ACKNOWLEDGMENTS

One of the authors (P. P. Jiang) would like to thank Dr. Wei Bai for providing the sample and Dr. Ting Huang for the constructive discussions. This work was financially supported by Major State Basic Research Development Program of China (Grant Nos. 2011CB922200 and 2013CB922300),

Natural Science Foundation of China (Grant Nos. 11374097, 61376129, and 11074076), Projects of Science and Technology Commission of Shanghai Municipality (Grant Nos. 13JC1402100 and 13JC1404200), and the Program for Professor of Special Appointment (Eastern Scholar) at Shanghai Institutions of Higher Learning.

[1]C. A. P. de Araujo, J. D. Cuchiaro, L. D. McMillan, M. Scott, and J. F. Scott, Nature (London) **374**, 627 (1995).
[2]T. Goto, T. Kimura, G. Lawes, A. P. Ramirez, and Y. Tokara, Phys. Rev. Lett. **92**, 257201 (2004).
[3]A. Srinivas, D. W. Kim, K. S. Hong, and S. V. Suryanarayana, Appl. Phys. Lett. **83**, 2217 (2003).
[4]P. F. Zhang, N. Deepak, L. Keeney, M. E. Pemble, and R. W. Whatmore, Appl. Phys. Lett. **101**, 112903 (2012).
[5]L. Sagalowicz, F. Chu, P. D. Martin, and D. Damjanovicd, J. Appl. Phys. **88**, 7258 (2000).
[6]J. M. Perez-Mato, P. Blaha, K. Schwarz, M. Aroyo, D. Orobengoa, I. Etxebarria, and A. Garcia, Phys. Rev. B **77**, 184104 (2008).
[7]C. H. Hervoches, J. T. S. Irvine, and P. Lightfoot, Phys. Rev. B **64**, 100102 (2001).
[8]C. H. Hervoches, A. Snedden, R. Riggs, S. H. Kilcoyne, P. Manuel, and P. Lightfoot, J. Solid State Chem. **164**, 280 (2002).
[9]M. Krzhizhanovskaya, S. Filatov, V. Gusarov, P. Paufler, R. Bubnova, M. Morozov, and D. C. Meyer, Z. Anorg. Allg. Chem. **631**, 1603 (2005).
[10]A. Snedden, C. H. Hervoches, and P. Lightfoot, Phys. Rev. B **67**, 092102 (2003).
[11]F. Kubel and H. Schmid, Ferroelectrics **129**, 101 (1992).
[12]S. Logothetidis, J. Petalas, M. Cardona, and T. D. Moustakas, Phys. Rev. B **50**, 18017 (1994).
[13]L. Viña, S. Logothetidis, and M. Cardona, Phys. Rev. B **30**, 1979 (1984).
[14]Z. H. Duan, Z. G. Hu, K. Jiang, G. S. Wang, X. L. Dong, and J. H. Chu, Appl. Phys. Lett. **102**, 151908 (2013).
[15]G. Chen, W. Bai, L. Sun, J. Wu, Q. Ren, W. Xu, J. Yang, X. J. Meng, X. D. Tang, C. G. Duan, and J. H. Chu, J. Appl. Phys. **113**, 034901 (2013).
[16]X. Chen, P. P. Jiang, Z. H. Duan, Z. G. Hu, X. F. Chen, G. S. Wang, X. L. Dong, and J. H. Chu, Appl. Phys. Lett. **103**, 192910 (2013).
[17]E. D. Palik, *Handbook of Optical Constants of Solids* (Academic Press, New York, 1991).
[18]P. Lautenschlager, M. Garriga, L. Viña, and M. Cardona, Phys. Rev. B **36**, 4821 (1987).
[19]R. V. Pisarev, A. S. Moskvin, A. M. Kalashnikova, and T. Rasing, Phys. Rev. B **79**, 235128 (2009).
[20]W. Bai, Y. Q. Gao, J. Y. Zhu, X. J. Meng, T. Lin, J. Yang, Z. Q. Zhu, and J. H. Chu, J. Appl. Phys. **109**, 064901 (2011).
[21]D. J. Singh, S. S. A. Seo, and H. N. Lee, Phys. Rev. B **82**, 180103 (2010).
[22]J. B. Li, Y. P. Huang, G. H. Rao, G. Y. Liu, J. Luo, J. R. Chen, and J. K. Liang, Appl. Phys. Lett. **96**, 222903 (2010).
[23]J. Ilczuk, D. Machura, and J. Rymarczyk, Mol. Quant. Acoust. **28**, 107 (2007).
[24]E. Buixaderas, I. Gregora, J. Hlinka, J. Dec, and T. Łukasiewicz, Phase Transitions **86**, 217 (2013).
[25]W. Wang, S. P. Gu, X. Y. Mao, and X. B. Chen, J. Appl. Phys. **102**, 024102 (2007).
[26]K. Jiang, W. W. Li, X. G. Chen, Z. N. Zhan, Z. G. Hu, and J. H. Chu, J. Raman Spectrosc. **43**, 583 (2012).
[27]J. J. Zhu, W. W. Li, G. S. Xu, K. Jiang, Z. G. Hu, and J. H. Chu, Acta Mater. **59**, 6684 (2011).